Measurements of Skin-friction of Systematically Generated Surface Roughness

Julio M. Barros
Department of Mechanical Engineering
United States Naval Academy
590 Holloway Rd, Annapolis, MD - 21402 USA
barros@usna.edu

Michael P. Schultz
Department of Naval Architecture and Ocean Engineering
United States Naval Academy
590 Holloway Rd, Annapolis, MD - 21402 USA
mschultz@usna.edu

Karen A. Flack
Department of Mechanical Engineering
United States Naval Academy
590 Holloway Rd, Annapolis, MD - 21402 USA
flack@usna.edu

ABSTRACT

Understanding the relationship between a surface's topography and its hydraulic resistance is an important, yet elusive, goal in fluids engineering. Particularly poorly understood are the flow conditions at which a given surface will begin to show the effects of roughness in the form of increased wall shear stress above that of the hydraulically smooth wall and the behavior of frictional drag in the transitionally rough regime. From a practical standpoint, the engineering correlations for the prediction of frictional drag should be based on information that can be obtained solely from the surface topography, thus excluding any information that requires hydrodynamic testing. Previous results (Flack & Schultz, 2010) have shown that the root-mean-square roughness height (k_{rms}) and the skewness (*Sk*) of the probability density function are the roughness scales that best predict frictional drag in the fully rough regime. The goal of this work is to take a systematic approach when generating surface roughness where the roughness parameters can be controlled. Three surfaces with fixed amplitude and varying power-law spectrum slope ($E(\kappa) \sim \kappa^P$; $P = -0.5, -1.0, -1.5$) were generated and replicated using high-resolution 3d printing. Results show that the surface with the shallower slope, $P = -0.5$, produces the highest drag, whereas the surface with the steeper slope, $P = -1.5$ produces the least drag. This highlights that some roughness scales do not contribute significantly to the drag. In fact, the effective slope, *ES* of the investigated surfaces were less that 0.35, which indicates that the surfaces are in the so-called "wavy" regime (Schultz & Flack, 2009). A high-pass filter of 1 mm (corresponding to ~ 10 times of the roughness height) was applied. By removing the long-wavelength roughness scales, the correlation between the equivalent sand-grain roughness, k_s and roughness root-mean-square, k_{rms} had the positive trend, whereas the unfiltered correlation provided a negative trend.

INTRODUCTION

Surface roughness is encountered in a multitude of practical and industrial applications, such as flow inside pipelines or over turbine blades (which may degrade with deployment time), and flow over complex geometries and/or topographies, such as urban and environmental flows. It is widely known that roughness increases frictional drag, which may lead to higher thermal loads and degradation of performance. Recently tested roughness was seen to cause additional undesirable effects in certain conditions, such as secondary flow (Barros & Christensen, 2014; Kevin *et al.*, 2017; Anderson *et al.*, 2015; Nugroho *et al.*, 2013), which may lead to lateral drag (Willingham *et al.*, 2014). Given the complexity of rough-wall flows, it is often desired to develop simple models based upon surface topography (i.e., roughness statistics, such as, root-mean-square, *rms*, skewness, *Sk*, kurtosis, *Ku*, etc.) to predict frictional drag in these engineering applications. Therefore, it is crucial to understand the relationship between surface's topography and its impact on the hydraulic resistance. One example would be the characterization of drag penalties due to different biofouling conditions on ship hulls. A particular advantage for having a simple drag predictive model based upon the roughness statistics would be the optimization between drag penalties (and thus a reduction in ship's performance and cruising speeds) and fuel/cleaning costs.

Many important studies have been conducted on simplified, sparse arrays of roughness elements, such as cubes and transverse square bars, which often have a single roughness scale, in order to develop correlations between drag penalties (more specifically, the roughness function, ΔU^+) and some roughness parameters. These parameters range from simple ones, such as roughness spacing parameter, λ = pitch/height (Bettermann, 1965) and the density parameter, λ_d = total surface area/total roughness area (Dvorak, 1969), to more complex ones, such as the combined density and shape parameter, $\Lambda = (d/k)(A_f/A_s)^{-4/3}$, where d is average element spacing, k is the roughness height, A_f is the frontal area of a single roughness element, and A_s is the windward wetted surface area of a single roughness element (Dirling, 1973). Macdonald *et al.* (1998) introduced an analytical model to predict drag, in the form of surface roughness height, z_0 (similar to the equivalent sand-grain roughness height, k_s), for staggered and square array of cubes. This model agrees very well with experimental data for a wide range of planform densities, $\lambda_p = A_p/A_d$, where A_p is the total plan area and A_d it the total area covered by the roughness elements. Recently, Yang *et al.* (2016) proposed a new analytical model for cubes (staggered and square arrays), where an exponential mean velocity profiles is assumed in the roughness layer, as evidenced in LES results presented in their work. Additionally, this model takes into account volumetric sheltering effects due to the momentum deficit in the wake of the roughness elements, which is accounted for in the drag on adjacent elements. Good agreement was found between their LES results and the Macdonald *et al.* (1998) analytical model.

As was previously mentioned, many practical roughness embody a multitude of roughness scales, and therefore cannot be easily characterized by the parameters described above. In addition, these practical, realistic roughness usually cover the entire surface, which, again, limits the use of parameters based on element to element spacing. Therefore, any predictive model for the frictional drag on these realistic surfaces have to rely upon surface statistics. Flack & Schultz (2010), using a multitude of roughness statistics data ranging from sandpaper with various grit scales to pyramids and packed spheres, developed a predictive model for k_s that is solely based upon the roughness root-mean-square height, k_{rms}, and the skewness of the probability density function, Sk, in the form of,

$$k_{s,\ \text{predicted}} = A\, k_{rms}(1+Sk)^b \tag{1}$$

where A and b are determined from a least square fit. It should be noted that this model only applies in the fully-rough regime. If fact, developing a model that covers all regimes - that is, hydraulically smooth to transitionally rough and fully-rough regimes, has proven to be challenging. Flack *et al.* (2016) generated 15 surfaces via grit-blasting, with various media sizes and combinations of thereof, and the skin friction was measured for a wide range of Reynolds numbers, covering all roughness regimes. They showed that the roughness function, ΔU^+ remains largely invariant with surface texture. One possible reason why these surfaces did not display significant differences in the transitionally rough regimes could be linked to Sk, which for all the tested surfaces were inherently negative. Additionally, for the surfaces which achieved fully-rough regime the k_s predicted by Flack & Schultz (2010) model matched quite closely with the ones measured experimentally, however with different constants from the aforementioned work.

Based upon the work from Flack *et al.* (2016), the current work takes a systematic approach, which consist of mathematically generating surfaces roughness where the roughness statistical parameters can be controlled. As an initial effort, three surface were created where the amplitude of the roughness was nominally kept constant coupled with a systematic variation of the power-spectrum density. The reproduction of these surfaces was done via high-resolution 3d printing, and subsequent hydrodynamics tests were performed in a channel flow facility where the skin friction was measured.

EXPERIMENTAL FACILITIES AND METHODS

The present experiments were conducted in the high Reynolds number turbulent channel flow facility at the United States Naval Academy. The test section is 25 mm in height (H), 200 mm in width (W), and 3.1 m in length (L). The bulk mean velocity in the test section ranges from 0.4 - 11.0 m/s, resulting in a Reynolds number based on the channel height and bulk mean velocity (Re_m) range from 10,000 - 300,000. Further details of the facility including flow managements devices, tripping, and flow quality are given in Schultz & Flack (2013). Nine static pressure taps are located in the test section of the channel. They are 0.75 mm holes and are placed along the centerline of the side wall of the channel and are spaced 6.8H apart. Pressure taps 5 - 8 are used to measure the streamwise pressure gradient in the channel, located $\sim 90H$ - $110H$ downstream of the trip at the inlet to the channel.

The wall shear stress, τ_w, is determined via measurement of the streamwise pressure gradient, dp/dx. The flow develops over smooth walls for a distance of $60H$ in the upstream portion of the channel. The roughness-covered plates form the top and bottom walls for the remainder of the test section. There is a roughness fetch of $30H$ before the first tap used in the determination of dp/dx. Fully-developed flow was confirmed with velocity profiles located $90H$ and $110H$ downstream of the trip. Details of the velocity measurements are outlined in Schultz & Flack (2013)

The rough surfaces investigated in this work are generated mathematically so the surface statistics can be systematically changed and controlled to identify the roughness scales that contribute the most to frictional drag. The surfaces were generated in MATLAB using a circular Fast Fourier Transform (FFT) with a random set of independent phase angles, distributed between 0 and 2π, with a power-law slope transfer function, $H = \kappa^P$, where κ is the wavenumber and P the slope of the power-law. This approach is similar to the one used by Anderson & Meneveau (2011). Therefore, the roughness generated by this method contains a multitude of scales that obeys the imposed power-law slope power spectrum ($E(\kappa) \sim \kappa^P$), and the surface elevation possesses a Gaussian probability-density-function (*p.d.f*). For the surface roughness tested in this work, the slope of the power law was systematically changed while holding the amplitude constant. Table 1 summarizes the surface statistics of the three tested surfaces, $P = -0.5, -1.0$ and -1.5. The generated surfaces were then reproduced using a high-resolution 3D printer (Projet 3500 HDMax, with lateral resolution 34μm, elevation resolution 16μm). To efficiently reproduce the printed rough surfaces, a mold/cast technique was employed. The silicon rubber molds were reinforced with 2 layers of carbon fiber to minimize any distortions to ensure that all roughness tiles had the same dimensions.

The surfaces scans, comprised of 50 mm by 15 mm (x and y direction, respectively), were profiled with an optical profilometer utilizing white light interferometry (Veeco Wyco NT9100), with sub-micron vertical resolution and 3.4μm of lateral resolution. Figure 8(left-panel) shows the contour maps of the investigated surfaces measured by the profilometer. The data acquired from the profilometer requires careful post-processing in order to remove any anomalies and spurious data as well as filling all holes in the surface scans. The surface scans had tilt and curvature removed, and the holes were filled using a PDE-based interpolation method (Bertalmio *et al.*, 2000). Spurious data from the interpolation step were removed by a median-test filter, followed by a second PDE-based interpolation. Further details of the post-processing can be found in Flack *et al.* (2016). In order to compute the roughness statistics, a total of 10 line-scans per surface were extracted (x - direction). These profiles had 1 mm space between them to ensure statistical independence.

RESULTS AND DISCUSSION

The skin-friction, C_f, results for all the tested surfaces as a function of Reynolds number, Re_m are shown in figure 2. Also shown are the smooth wall experimental results of Schultz & Flack (2013) for comparison. At lower Reynolds number, all surfaces are hydraulically-smooth. Furthermore, at sufficiently high Reynolds number the surfaces exhibit fully rough behavior, where the skin friction becomes independent of Reynolds number. Surface 1 ($P = -0.5$) produces the highest frictional drag, whereas surface 3 ($P = -1.5$) has the lowest drag. This is an interesting result, because as the power-law slope, P, becomes steeper the surface tends to produce less drag. This seems counterintuitive if one only draws a conclusion regarding the drag from the surfaces' statistics (table 1) and surface topography maps (figure 8). In fact, it is clear that the surface with the power-law slope of $P = -1.5$ has the largest statistical and topographical features, whereas the surface with the slope of $P = -0.5$ has the least. Conversely, table 1 shows that the equivalent roughness grain height, k_s, for $P = -0.5$ is $k_s = 53.0\mu$m (most drag), and $k_s = 21.0\mu$m for $P = -1.5$ (least drag). The results from the skin-friction seems to indicate that there are roughness scales that do not contribute significantly to the drag.

The roughness function, ΔU^+, for a range of roughness Reynolds number, k_s^+, where k_s is the equivalent sand grain rough-

Table 1. Roughness statistics of the tested surfaces.

Surface	$E(\kappa) \sim \kappa^P$	$k_a [\mu m]$	$k_{rms} [\mu m]$	$k_t [\mu m]$	Sk	Ku	ES	$k_s [\mu m]$
1	$P = -0.5$	21.0	25.9	73.3	0.11	2.9	0.14	53.0
2	$P = -1.0$	25.3	31.1	84.9	0.08	2.9	0.12	33.5
3	$P = -1.5$	24.3	40.4	104.2	-0.03	2.9	0.09	21.0

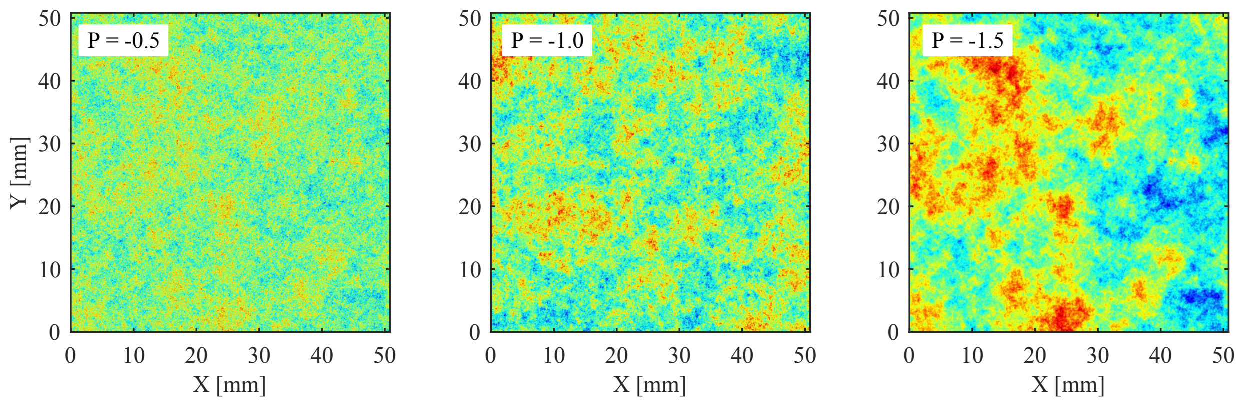

Figure 1. Mathematically generated rough surfaces with power law slopes $P = -0.5, -1.0$ and -1.5.

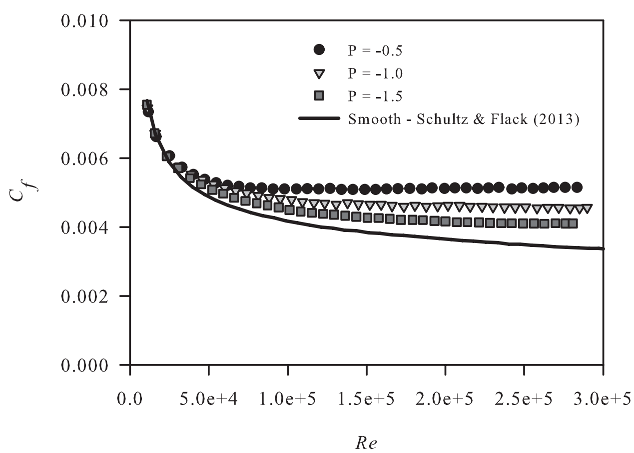

Figure 2. Skin-friction coefficient.

ness height, is shown in figure 3. A similarity-law procedure of Granville (1987) for fully-developed internal flows was employed to determine the roughness function, ΔU^+. In the fully-rough regime the roughness function for all the tested surfaces display good collapse, as expected, when scaled with using k_s. The onset to the transitionally-rough regime seems to be a function of the power-law slope, P, where it varies from $k_s^+ \sim 0.7$ for $P = -1.5$ to $k_s^+ \sim 2$ for $P = -0.5$. Additionally, the onset of the fully rough regime occurs from $k_s^+ \sim 10$ to $k_s^+ \sim 15$, and it also seems to be a function of the power-law slope. Therefore, the rough surfaces tested in this work display variations in the transitionally-rough regime. This is particularly interesting because in a previous study from Flack *et al.* (2016) they found that the different grit-blasted surfaces did not display significant variations in the transitionally-rough regime. In fact, the roughness function remained relatively invariant with surface texture. This may have to do with the fact that these grit-blasted surfaces are inherently positively skewed, similarly with the sand-roughness investigated by Nikuradse (1933). It is important to remember that the surfaces tested in this work have Gaussian *p.d.f* ($Sk \sim 0$; $Ku \sim 3$). Therefore, it could be that skewness may play an important role in the overall behavior of the roughness function in the transitionally-rough regime.

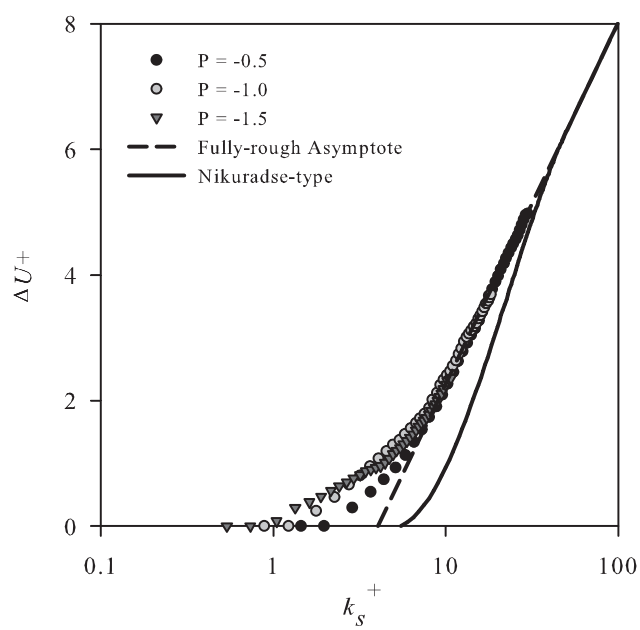

Figure 3. Roughness function.

As previously mentioned, it seems that there may be some roughness scales, mainly in the $P = -1.5$ and $P = -1.0$ cases, that do not significantly contribute to frictional drag. Referring back to figure 8, one could naively draw conclusions regarding the impact each of surfaces tested herein have on the drag by simply looking at their topographical features, i.e. how rough they are.

Figure 4(a) shows the correlation between the effective slope, ES, and the roughness function for the tested roughness. Additionally, data from Napoli *et al.* (2008) and Schultz & Flack (2009) are included for comparison. It can be seen that the surface roughness investigated in this work fall bellow the value where the roughness function is independent of the effective slope, $ES \geq 0.35$. This means that the tested roughness fall under the so-called "wavy" regime (Schultz & Flack, 2009). The implication of this factor is that long wavelength roughness scales may not play an important role in generating drag.In fact, Schultz & Flack (2009) pointed out that for surfaces with $ES \leq 0.35$ the roughness height does not provide a good scale for the roughness function. This may help explain why surface 1 ($P = -0.5$) produces higher drag than surface 3 ($P = -1.5$), where, clearly, the latter possesses more dominantly long wavelength roughness scales. Additionally, It is worth noting that effective slope has a Reynolds number dependency, as depicted in figure 4(b) (data available for the current work and Schultz & Flack (2009)).

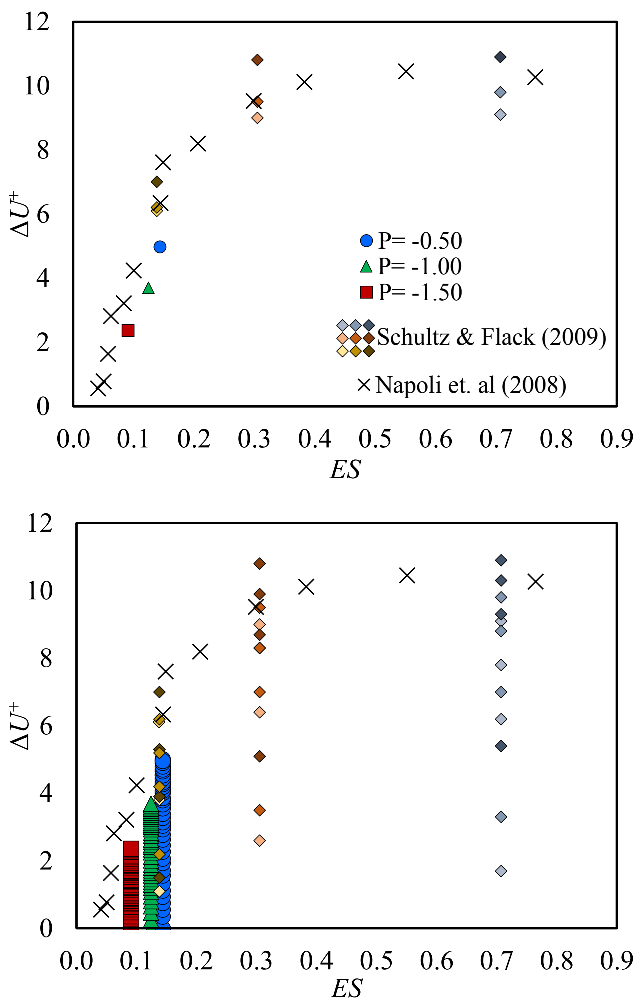

Figure 4. Effective slope, ES, *versus* roughness function, ΔU^+, for the tested surfaces (colored ○ symbols), (a) Highest Reynolds number, and (b) Reynolds number dependency. Also included Napoli *et al.* (2008) (× symbols), and Schultz & Flack (2009) (colored ◇ symbols)

It is, therefore, important to identify which scales are contributing more to the generation of frictional drag. In order to determine the threshold of which the longer wavelength scales start to not have a significant role on the drag, a high-pass filter was applied on the profiled surface data for all the three tested roughness. To determine the size of the filter, the R^2 value was computed from a linear least-square fit between high-pass filtered roughness root-mean-square, k_{rms}, and k_s, for a range of filter size (from 0.1 mm to 10 mm). This resulted in a optimal filter size of 1 mm, where this values is approximately 10 times higher than the largest surface statistic (roughness peak-to-trough height, k_t for the surface 3). Subsequently, the roughness statistics were computed for this filter size. Figure 5 shows the correlation between k_{rms} and k_s for both unfiltered and with a 1 mm high-pass filter applied. It is clear that, for the unfiltered roughness statistics, the correlation between k_{rms} and k_s has an opposite trend when compared with the k_s trend, that is, when k_s is higher, i.e. more drag, k_{rms} is smaller. This is clearly counterintuitive. Conversely, when a 1 mm high-pass filter was applied to the tested surfaces, the correlation between k_{rms} and k_s has the correct trend, that is, when k_{rms} becomes higher k_s also increases. The same trend can be observed for other surface statistics (e.g, roughness average height, k_a and k_t; not shown here for brevity). Interestingly, the values of ES for both unfiltered and 1 mm high-pass filtered surfaces remain relatively unchanged (figure 6). This means that ES is quite insensitive to high-pass filtering, and thus a potential robust parameter candidate for future roughness models. In fact, Chan *et al.* (2015) developed a model for ΔU^+ as a function of solely k_a^+ (normalized in inner wall units) and ES from DNS over 3D sinusoidal-type roughnesses. The data from Napoli *et al.* (2008); Yuan & Piomelli (2014) and Schultz & Flack (2009) were also used in this model resulting in a good agreement with the measured ΔU^+.

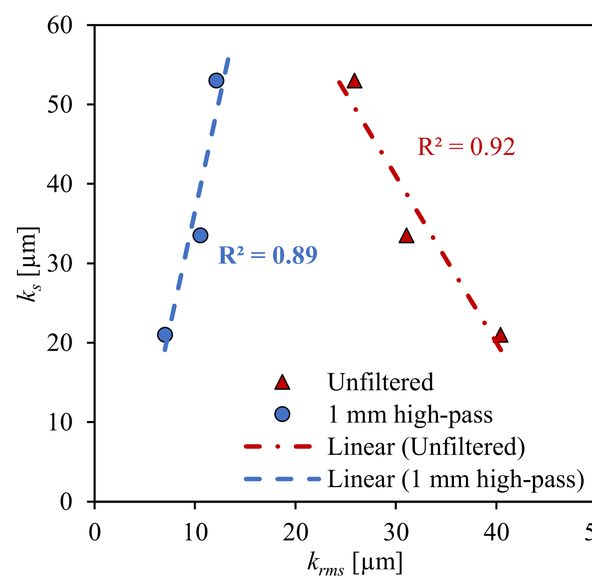

Figure 5. Correlation between k_{rms} and k_s for unfiltered and for 1 mm high-pass filter.

The model proposed by Flack & Schultz (2010) was employed for both the unfiltered and 1 mm high-pass filtered statistics, as shown in figure 7. It can be seen that the model provides the same correct trend for both statistics. However, the determined coefficients are vastly different. Although, the coefficients for the filtered statistics data more closely match the ones determined in Flack & Schultz (2010). It is worth noting that the 1 mm high-pass filter fit

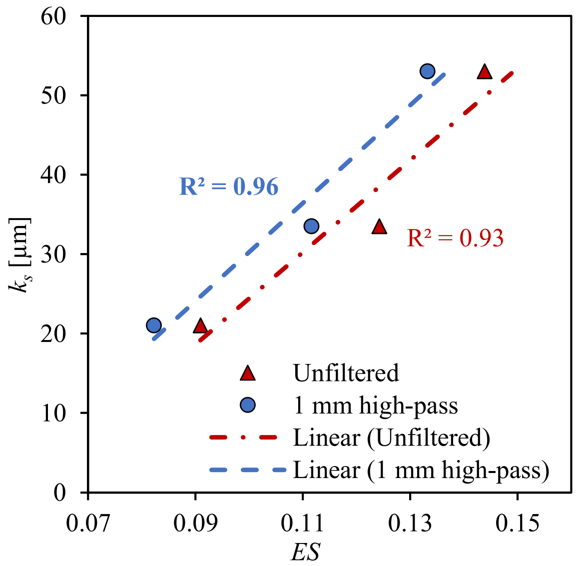

Figure 6. Correlation between ES and k_s for unfiltered and for 1 mm high-pass filter.

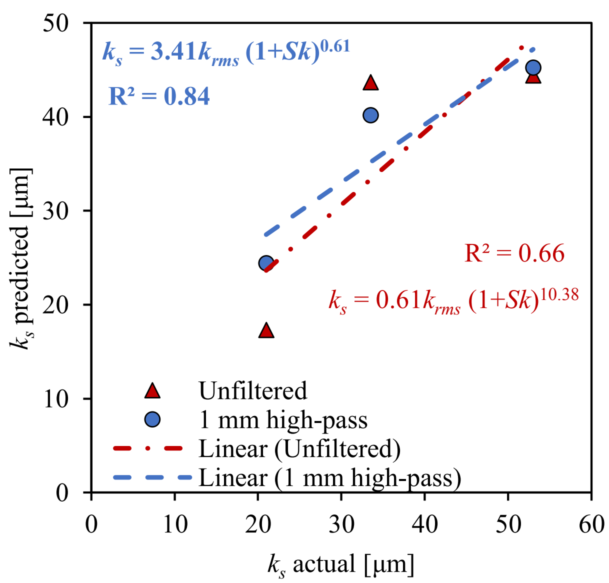

Figure 7. Correlation between k_s actual and k_s predicted by Flack & Schultz (2010) model for unfiltered and for 1 mm high-pass filter.

provides a better R^2. Moreover, ideally, more roughness data are needed to fully asses this model in the so-called "wavy-regime". However, as a first order analysis this result further emphasizes the necessity of surface filtering in order to identify the scales that contribute more towards frictional drag.

Finally, to qualitatively demonstrate the effect of the high-pass filter has on the tested surfaces, figure 8 depicts the contour maps of the measured roughness, where the left panel shows the original, unfiltered data from the profilometer (with both curvature and tilt removed) and the right panel shows the surfaces in which the 1 mm high-pass filter was applied. Focusing on the high-pass filtered contour maps (right panel), it can be seen that surface with $P = -0.5$ has the most topographical features, whereas the surface with $P = -1.5$ has the least features, with surface $P = -1.0$ siting in between. As expected, this qualitatively result has the exact trend seen on the frictional drag curves (figure 2). It is particularly interesting to see what roughness scale are contributing to the frictional drag, which provides a link between the trends seen in the C_f curves coupled with the justification for filtering the surfaces based on the fact that their effective slope values fall in the "wavy" regime with $ES \leq 0.35$.

SUMMARY

Results are presented for three rough surfaces with a range of scales following a power-law slope of $P = -0.5$, -1.0 and -1.5. Skin friction for all tested surfaces display fully-rough behavior and the entire roughness function is mapped to determine the extent and shape of ΔU^+ in the transitionally rough regime. Interestingly, the surface with power law slope $P = -0.5$ generate the most drag even though this surface has the smallest roughness features as determined from surface statistics. As the power law slope increases, the drag imposed by the surfaces is reduced. This emphasizes that some surface wavelengths are not significantly contributing to the drag. These are likely the undulating, wavy surface features. In fact, the ES of all the surfaces fall under the so-called "wavy" regime. These results highlight the need for high-pass filtering in the determination of predictive correlations for frictional drag, which produce the correct trend between k_s and k_{rms}.

REFERENCES

Anderson, W., Barros, J. M., Christensen, K. T. & Awasthi, A. 2015 Numerical and experimental study of mechanisms responsible for turbulent secondary flows in boundary layer flows over spanwise heterogeneous roughness. *Journal of Fluid Mechanics* **768**, 316–347.

Anderson, W. & Meneveau, C. 2011 Dynamic roughness model for large-eddy simulation of turbulent flow over multiscale, fractal-like rough surfaces. *Journal of Fluid Mechanics* **679**, 288–314.

Barros, J. M. & Christensen, K. T. 2014 Observations of turbulent secondary flows in a rough-wall boundary layer. *Journal of Fluid Mechanics* **748**, R1.

Bertalmio, M., Sapiro, G., Caselles, V. & Ballester, C. 2000 Image inpainting. In *Proceedings of the 27th Annual Conference on Computer Graphics and Interactive Techniques*, pp. 417–424. ACM Press/Addison-Wesley Publishing Co.

Bettermann, D. 1965 Contribtion a l'etude de la couche limite turbulent le long de plaques regueuses. *Tech. Rep.* 65-6. Center National de la Recherche Scientifique.

Chan, L., MacDonald, M., Chung, D., Hutchins, N. & Ooi, A. 2015 A systematic investigation of roughness height and wavelength in turbulent pipe flow in the transitionally rough regime. *Journal of Fluid Mechanics* **771**, 743–777.

Dirling, Jr, R. 1973 A method for computing roughwall heat transfer rates on reentry nosetips. In *8th Thermophysics Conference*, p. 763.

Dvorak, F. 1969 Calculation of turbulent boundary layers on rough surfaces in pressure gradient. *AIAA journal* **7** (9), 1752–1759.

Flack, K. A. & Schultz, M. P. 2010 Review of hydraulic roughness scales in the fully rough regime. *Journal of Fluids Engineering* **132** (4), 041203.

Flack, K. A., Schultz, M. P., Barros, J. M. & Kim, Y. C. 2016 Skin-friction behavior in the transitionally-rough regime. *International Journal of Heat and Fluid Flow* **61**, 21–30.

Granville, P. S. 1958 The frictional resistance and turbulent boundary layer of rough surfaces. *Journal of Ship Resistance* **2**, 52–74.

Granville, P. S. 1987 Three indirect methods for the drag characterization of arbitrarily rough surfaces on flat plates. In *Proceedings of the Twenty-first American Towing Tank Conference*, p. 117. National Academies.

Kevin, K., Monty, J. P., Bai, H. L., Pathikonda, G., Nugroho, B.,

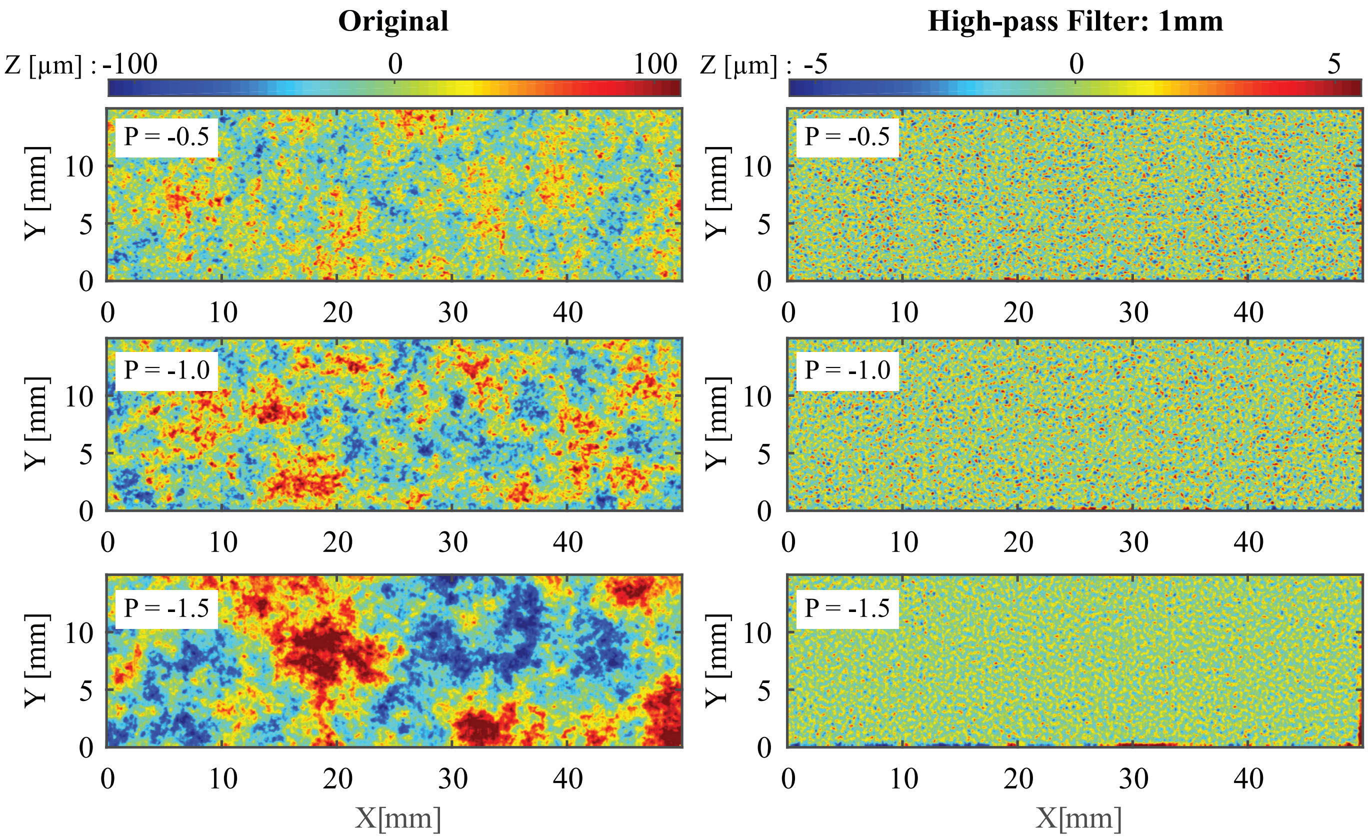

Figure 8. Contour maps of digital scans for all three tested surface roughness. Left panel shows the surfaces without filtering, whereas the right panel shows the surfaces with a 1 mm high-pass filter.

Barros, J. M., Christensen, K. T. & Hutchins, N. 2017 Cross-stream stereoscopic particle image velocimetry of a modified turbulent boundary layer over directional surface pattern. *Journal of Fluid Mechanics* **813**, 412–435.

Macdonald, R., Griffiths, R. & Hall, D. 1998 An improved method for the estimation of surface roughness of obstacle arrays. *Atmospheric Environment* **32** (11), 1857–1864.

Napoli, E., Armenio, V. & De Marchis, M. 2008 The effect of the slope of irregularly distributed roughness elements on turbulent wall-bounded flows. *Journal of Fluid Mechanics* **613**, 385–394.

Nikuradse, J. 1933 Laws of flow in rough pipes. *NACA Technical Memorandum 1292* .

Nugroho, B., Hutchins, N. & Monty, J. 2013 Large-scale spanwise periodicity in a turbulent boundary layer induced by highly ordered and directional surface roughness. *International Journal of Heat and Fluid Flow* **41**, 90–102.

Schultz, M. P. & Flack, K. A. 2009 Turbulent boundary layers on a systematically varied rough wall. *Physics of Fluids* **21** (1), 015104.

Schultz, M. P. & Flack, K. A. 2013 Reynolds-number scaling of turbulent channel flow. *Physics of Fluids* **25** (2), 025104.

Willingham, D., Anderson, W., Christensen, K. T. & Barros, J. M. 2014 Turbulent boundary layer flow over transverse aerodynamic roughness transitions: induced mixing and flow characterization. *Physics of Fluids* **26** (2), 025111.

Yang, X. I., Sadique, J., Mittal, R. & Meneveau, C. 2016 Exponential roughness layer and analytical model for turbulent boundary layer flow over rectangular-prism roughness elements. *Journal of Fluid Mechanics* **789**, 127–165.

Yuan, J. & Piomelli, U. 2014 Estimation and prediction of the roughness function on realistic surfaces. *Journal of Turbulence* **15** (6), 350–365.